Mechanism of the Vanadium Oxide-Catalyzed Selective Reduction of NO by NH_3. A Quantum Chemical Modeling

F. Gilardoni,[†] J. Weber,*[,†] and A. Baiker[‡]

Department of Physical Chemistry, University of Geneva, 30 Quai Ernest-Ansermet, CH-1211 Genève 4, Switzerland, and Department of Chemical Engineering and Industrial Chemistry, Swiss Federal Institute of Technology, ETH-Zentrum, CH-8092 Zuerich, Switzerland

Received: January 9, 1997; In Final Form: June 4, 1997[⊗]

Quantum chemical calculations have been performed using density functional theory to model the mechanism of selective catalytic reduction of NO by NH_3 on vanadium oxide. The reaction is initiated by NH_3 adsorption on a Brønsted site modeled as a dimer cluster model representative of vanadium oxide, containing a terminal V═O adjacent to a V−OH group. The calculations indicate that the adsorbed NH_3 behaves as NH_4^+, which is supported by calculated IR spectra. Subsequently NO reacts with this activated NH_3 to yield NH_2NO and finally the reaction products N_2 and H_2O. The present results give support to a dual-site Eley−Rideal-type mechanism involving a Brønsted site and agree with isotopic labeling studies.

I. Introduction

Because of its environmental importance, the selective catalytic reduction (SCR) of NO_x by NH_3 has been extensively studied. Important features of the reaction have been summarized in reviews.[1] Among the various catalysts which are active in SCR of NO, vanadia-based catalysts are most widely applied due to their excellent activity, selectivity, and stability. Most of the industrial SCR catalysts contain the active vanadia dispersed on TiO_2, which proved to be the most suitable single oxide support material. Additional components used are SiO_2 for structural promotion and WO_3 for broadening the temperature range for reaction. In this light it is not surprising that most experimental studies on the reaction mechanism have been carried out either on titania-supported vanadia or on pure, unsupported vanadia catalysts. Different reaction mechanisms have been proposed and discussed in the literature.[1−11] Both the reaction mechanisms and the nature of the active vanadia sites are still debated.

It is generally accepted that the vanadium-catalyzed SCR of NO proceeds according to the following stoichiometry:

$$4NO + 4NH_3 + O_2 \rightarrow 4N_2 + 6H_2O$$

Several studies [2,3,9,12,13] revealed that ammonia adsorbs on both Brønsted acid sites (associated with V−OH surface groups) and Lewis acid sites (coordinated form) on vanadia−titania catalysts, which gave rise to different suggestions concerning the reaction mechanism. Based on IR spectroscopic studies, Takagi *et al.*[2,14] proposed a Langmuir−Hinshelwood-type mechanism involving NO, adsorbed as NO_2 (O_s + NO), and NH_3 adsorbed as NH_4^+. In contrast, Inomata *et al.*[3] deduced from gas chromatographic (GC) and IR spectroscopic investigations that NH_4^+ acts as the active ammonia species and reacts with gas phase NO according to an Eley−Rideal-type mechanism (ERM). Janssen *et al.*[15] further supported this mechanism by isotopic transient studies involving $^{18}O_2$ and $^{15}N_2$, which indicated that ammonia does not react with O_2 or O from any source during the reaction; nitrogen and nitrous oxide are produced by a reaction involving all three species: NO, NH_3, and/or O_2. Furthermore, it has been shown that, among the NH_3 and NO reactants, only NH_3 is strongly adsorbed.[16] Gasior *et al.*[4] concluded from both IR and XPS measurements on single-crystal surfaces of V_2O_5 that the SCR proceeds via participation of ammonia adsorbed on Brønsted acid sites. The important role of Brønsted acid sites in SCR of NO has been confirmed recently by in situ FTIR studies on titania-supported vanadia.[17−19] Odriozola *et al.*[6] showed by means of Auger electron spectroscopy and thermal desorption spectroscopy that NO adsorbs only on titania and on reduced vanadia, but not on oxidized vanadia surfaces. A similar behavior was found using positron-emitting ^{13}NO in SCR.[20]

According to Ramis *et al.*,[13] the reaction proceeds via ammonia adsorbed on Lewis sites of vanadia. This mechanism contrasts those described above, where ammonia bound to Brønsted sites was suggested to be crucial.

Although considerable experimental evidence is available concerning the initial step (ammonia adsorption) of SCR, the subsequent steps have not been clearly elucidated experimentally so far. Theoretical studies of the thermal deNO_x process[21−28] suggest the reaction of NH_2 with NO to be a primary product channel leading to N_2 and H_2O, where NH_2NO has been considered to be a crucial intermediate. The secondary products from this channel seem to be N_2H + OH,[21,23,24,28] which act as the chain-branching step allowing the process to proceed.[23,24,29−32]

The objective of the present study is to elucidate the role of the NH_2 + NO interaction in the heterogeneously catalyzed SCR process. This aim has been brought about by means of a density functional theory (DFT) investigation with special focus on (i) the reaction involving an activated NH_3[33] with an incoming NO and (ii) the potential energy surface of the adduct NH_2NO.

The finite cluster approximation to an infinite surface of a substrate is widely used in model studies of chemisorption/desorption processes in heterogeneous catalysis.[34−38] This approach is valid when the adsorbate creates rather short-range perturbation of a substrate, localized mainly on the active site responsible for substrate−adsorbate bonding. Assuming these conditions to prevail, a V_2O_9H cluster (see **1** in Figure 1) of C_s symmetry has been taken to model the surface, in which V atoms adjacent to the cluster were substituted by terminal H atoms. As compared to a full treatment of the bulk crystal or to the

* To whom correspondence should be addressed.
† University of Geneva. FAX: +41/22/702 65 18.
‡ Swiss Federal Institute of Technology. FAX: +41/1/632 11 63.
⊗ Abstract published in *Advance ACS Abstracts,* August 1, 1997.

S1089-5639(97)00160-6 CCC: $14.00

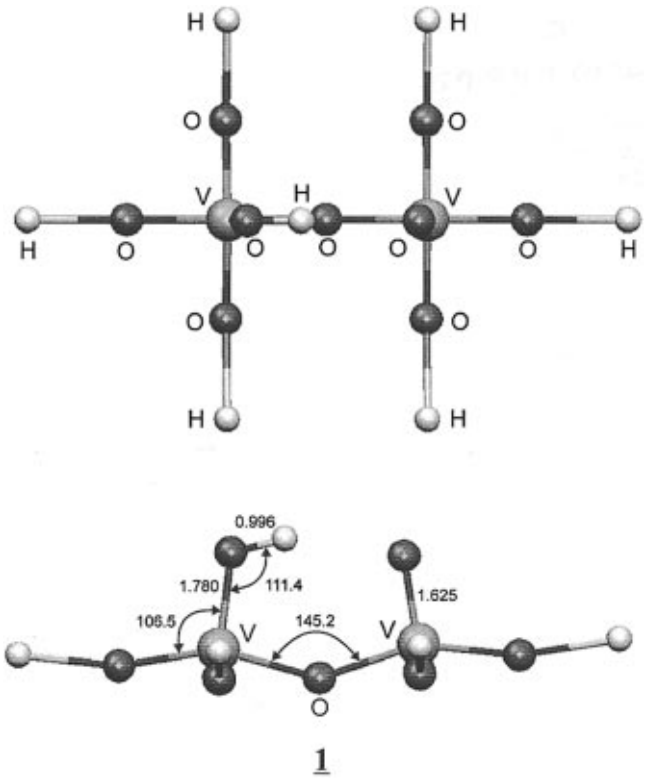

1

Figure 1. V_2O_9H cluster **1** used to model the interaction between NH_3 and V_2O_5 surfaces. Distances are in angstroms and angles in degrees.

use of embedded clusters, this approximate treatment can be justified as recently demonstrated by Witko *et al.*,[34] who showed that the electronic structure of the oxygen sites is not changed if the substrate cluster is increased beyond V_2O_9H. Further, saturation of the peripheral oxygen bonds by hydrogen has only a minor influence on the oxygen sites.[34,36] In a previous work,[33] we found that DFT calculations were able to reproduce accurately both the V═O and the V−OH bond lengths derived from experimental investigations.[39] We also showed that NH_3 may be adsorbed on V_2O_5 as a Brønsted-bound ammonia yielding **2a** and **2b** (Figure 2a,b), in agreement with experimental studies.[2,12,16−18] The chemisorption complex of NH_4^+ in **2a** has been found to be energetically favored by 14.2 kcal/mol compared to that in **2b**. The adsorption energy of NH_3 on V_2O_9H (25.0 kcal/mol) calculated in a previous study[33] agrees well with NH_3 desorption enthalpies derived from temperature-programmed desorption measurements (18−26 kcal/mol[19] and 22−28 kcal/mol[40]) carried out over vanadia- and titania-supported vanadia, suggesting nonactivated ammonia adsorption. Furthermore, we have also evidenced the distorted geometry of the chemisorbed ammonium ion.[33]

II. Computational Method

The linear combination of the Gaussian-type orbital-model core potential-density functional theory (LCGTO-MCP-DFT) method[41−44] and its corresponding deMon package[44] has been used. The nonlocal gradient corrections as suggested by Becke[45] for exchange and Perdew[46] for correlation functionals (BP86) have been used in this study. All the core and valence electrons were explicitly taken into account. The one-electron (orbital) basis set used in the calculations has been optimized for LCGTO-MCP-DFT by Godbout *et al.*[47] In our case, the V and H basis sets are of double-ζ plus polarization quality, and triple-ζ plus polarization quality for N and O, the contraction patterns being V(63321/531/41), H(41/1), N(5211/411/1), and O(5211/411/1), which leads in the usual six-component d-type Cartesian Gaussian functions to basis sets of dimension 254 for **1** (Figure 1), 288 for **1** + NH_3 (Figure 2a,b), and 326 for **1** + NH_3 + NO (Figure 3). The basis sets required by the LCGTO-DFT model to fit the electron density and the exchange−correlation potential have been chosen as V(5,5;5,5), H(5,1;5,1), N(5,2;5,2), and O(5,2;5,2).

Vibrational analyses were carried out analytically on the optimized structures **1**, **2a**, and **2b** derived from calculations using the Gaussian-94/DFT program package.[48] The 6-31G* (for H, N, O) and 6-311G** (for V) basis sets were used in these calculations. The starting geometry of the various species used to model the deNO_x process[33] has been taken from previous calculations performed with the deMon package. The structural parameters of the six coplanar O−H groups bonded to the vanadium atoms have been kept frozen. Each peak of the simulated IR spectra has been assumed to exhibit the shape of a Lorentzian curve in which the width at half-height has been taken equal to 4 cm^{-1}.

The potential energy surfaces of the initial adduct NH_2NO and its dissociation reactions have been investigated by using the Gaussian-94/DFT program package.[48] The 6-311++G** basis sets were used for H, N, and O, and extrafine integration grids have been taken in these calculations. The initial geometry of both intermediates and transition states of the relevant reaction steps were extracted from a previous work of Duan and Page.[21] In order to consistently explore the influence of the exchange−correlation part on the energetics, a set of three exchange−correlation functionals have been used: (i) the Becke's[49] three-parameter hybrid method using the Lee, Yang, and Parr correlation functional[50,51] (B3LYP), (ii) the Becke's 1988 exchange functional[45] and the Perdew and Wang's gradient-corrected correlation functional[52] (BPW91), and (iii) the BP86.[45,46]

The calculated harmonic frequencies have been compared with observed frequencies that contain anharmonic contributions. Neither the calculation of anharmonic vibrational energy levels nor experimental determination of harmonic frequencies is routinely practical for polyatomic molecules.[53−55] It requires detailed knowledge of both quadratic and anharmonic force constants, and it is only feasible for very small molecules.

III. Results and Discussion

The harmonic vibrational frequencies have been calculated analytically for **1**, **2a**, **2b**, NH_3, and NH_4^+. Both the ammonia and the ammonium ion were previously optimized at the same level of theory used for **1**, **2a**, and **2b**. The results are listed in Tables 1−4, and the simulated IR spectra are displayed in Figures 3 and 4. Structure **2a** exhibits harmonic frequencies that are all positive, whereas **2b** has one imaginary frequency (258i cm^{-1}), suggesting that **2a** is a local minimum and **2b** a transition state. The simulated IR spectra of **2a**, NH_3, and NH_4^+ have been superimposed in Figure 5. A comparison of these spectra with the in situ IR measured under reaction conditions supports the suggestion that the SCR reaction is initiated by NH_3 adsorption on a Brønsted acid site (V−OH).[17−19] Adsorbed ammonia is then activated by the transfer of H to an adjacent V^{5+}═O.[2,12,16−18] The present calculations agree with earlier experimental studies,[9] which uncovered a direct correlation between the concentration of the Brønsted acid sites and NO conversion, and they are consistent with the observed formation of new reduced V−OH species.[9,12]

In a subsequent step, efforts toward elucidating the reaction involving **2a** and an incoming NO have been undertaken. A plausible initial position of NO has been deduced by sampling the potential energy surface of **3** by performing single-point calculations. The resulting structure **4** is displayed in Figure 6. Then **4** has been optimized by freezing the structural parameters of (i) the oxygen atom bridging the two vanadyl

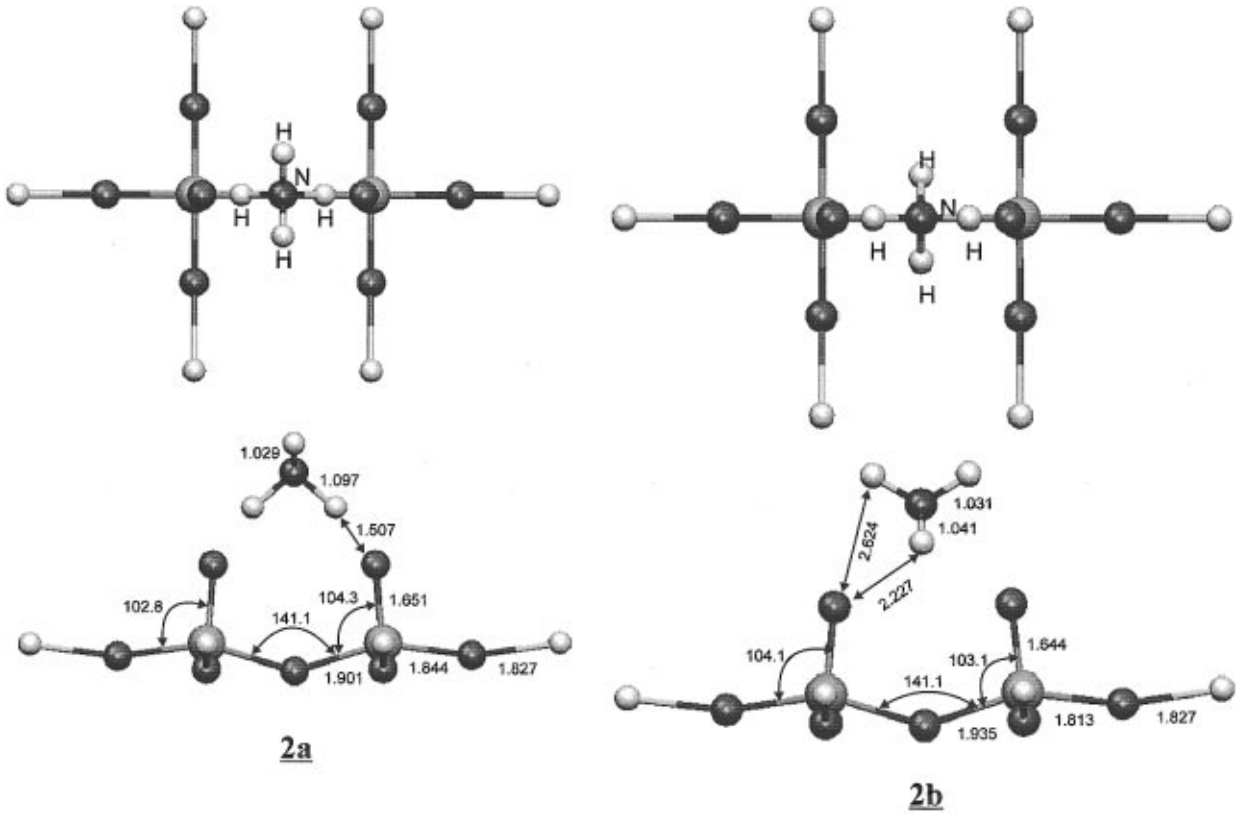

Figure 2. (a) NH_3 adsorption on **1**. The activated complex **2a** has a C_{2v} symmetry. Distances are in angstroms and angles in degrees. (b) Alternative NH_3 adsorption on **1**. The transition state **2b** has a C_{2v} symmetry. Distances are in angstroms and angles in degrees.

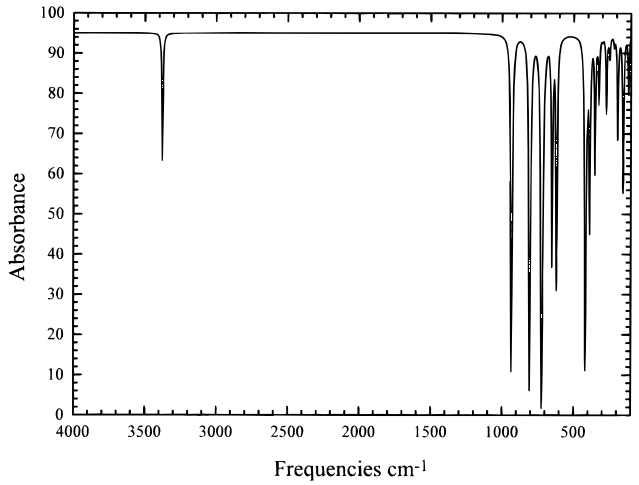

Figure 3. Simulated infrared spectrum of **1**. Each peak of the simulated IR spectra has been assumed to exhibit the shape of a Lorentzian curve in which the width at half-height has been taken equal to 4 cm^{-1}.

groups, (ii) the vanadium atoms, and (iii) the six planar O−H groups bonded to the vanadium centers. This led to the release of the adduct H_2NNO (*N*−nitrosamide) **lm.1** (local minimum) from a V^{4+}−OH moiety **5** as shown in Figure 7a,b. The heat of this reaction was found to be equal to +18.2 kcal/mol (+17.0 kcal/mol including the zero-point energies correction), corresponding to an endothermic process. Unfortunately, there are no experimental data of ΔH_0 for the formation of NH_2NO reported in the literature.[23] Note that no experimental evidence for the formation of NH_2NO has been found so far under the SCR conditions. However using a dual-vacuum chamber quadrupole mass spectrometer system Farber and Harris[56] observed NH_2NO as a major reaction product of the reaction of NH_3 and NO on a vanadium oxide catalyst at 300−400 °C. The formation of NH_2NO adduct with a minimum lifetime of

TABLE 1: IR Frequencies of the Activated Complex $NH_4V_2O_3(OH)_6$ 2a Calculated Using the Gaussian-94/DFT Program Package and BP86 Exchange−Correlation Functional

frequency (cm^{-1})	symmetry	intensity	mode description
3495	B1	w	ν_{asym} N−H_b[a]
3409	A1	w	ν_{sym} N−H_b[a]
2503	A1	vs	ν_{sym} N−H_a[b]
2228	B2	w	ν_{asym} N−H_a[b]
1663	A1	m	δ_{sym} N−H
1568	B1	w	γ_{sym} N−H
1483	A1	m	δ_{asym} N−H
1252	B2	w	γ_{sym} N−H
915	A1	m	δ_{sym} V═O
838	B2	vw	δ_{asym} V═O

[a] H pointing away from V═O. [b] H pointing to V═O.

TABLE 2: IR Frequencies of the Transition State $NH_4V_2O_3(OH)_6$ 2b Calculated Using the Gaussian-94/DFT Program Package and BP86 Exchange−Correlation Functional

frequency (cm^{-1})	intensity	frequency (cm^{-1})	intensity
3479	vw	1417	s
3423	w	1365	m
3303	vw	914	s
3272	m	627	m
2134	vs	258i	vw
1428	vw		

100 μs was suggested as a primary step in the reaction mechanism leading to N_2 and H_2O products.[56]

The V^{4+}−OH species can be reoxidized by either NO or O_2 to regenerate V^{5+}═O;[9,57] the reaction rate is enhanced in the presence of O_2.[16] Duffy *et al.*[57] showed that, in the absence of O_2, reoxidation must be accomplished by nitric oxide. The results of their isotope studies indicate that nitrogen atoms so released end up as ammonia; $^{15}NH_3$ is obtained by using ^{15}NO as an incoming species. The structural parameters and the corresponding simulated IR spectra of **5** are displayed in Figure

TABLE 3: IR Frequencies of NH_3 Calculated Using the Gaussian-94/DFT Program Package and BP86 Exchange−Correlation Functional

frequency (cm^{-1})	symmetry	intensity	mode description
3468	A1	vw	ν_{sym} N−H
3332	E	vw	ν_{asym} N−H
1686	A1	v	δ_d N−H
1116	E	vs	δ_s N−H

TABLE 4: IR Frequencies of NH_4^+ Calculated Using the Gaussian-94/DFT Program Package and BP86 Exchange−Correlation Functional

frequency (cm^{-1})	symmetry	intensity	mode description
3401	T2	s	ν_{asym} N−H
1482	T2	s	δ_d N−H

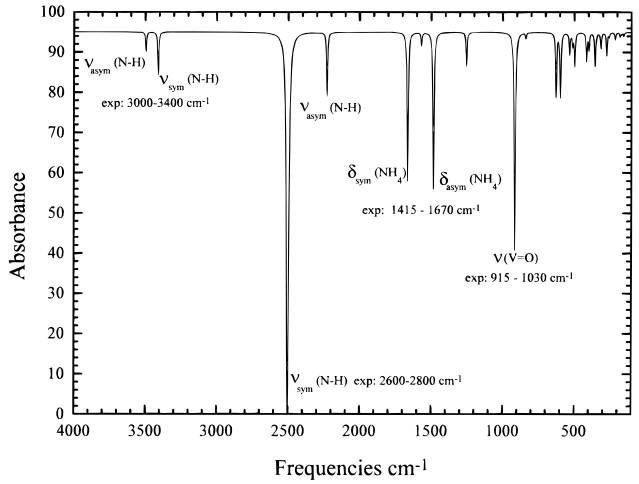

Figure 4. Simulated infrared spectrum of **2a**.

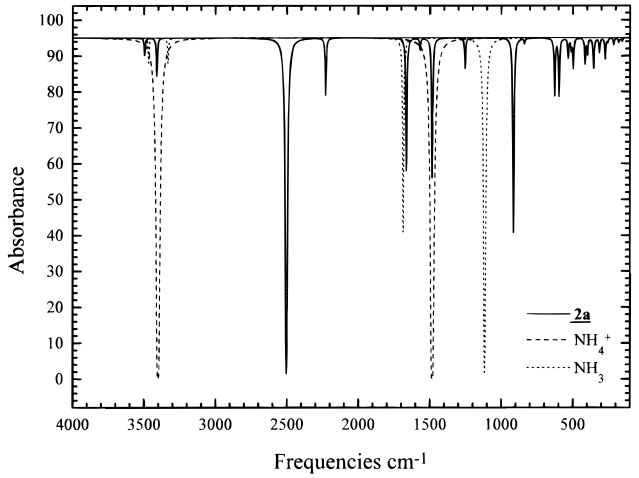

Figure 5. Superposition of simulated infrared spectra of **2a**, NH_3, and NH_4^+.

7b and Figure 8, respectively. These calculations indicate that (i) **5** is a local minimum (no imaginary frequency exhibited), (ii) neither V−OH_a nor V−OH_b exhibits structural or spectroscopic properties similar to those found for the vanadia hydroxyl group in **1**, (iii) H_b is stabilized by interaction with the lone pair of the oxygen atom bonded to H_a, (iv) H_a and H_b are drastically different, and (v) **5** does not release water spontaneously. The bond lengths differ by 0.062 Å for V−O and 0.028 Å for O−H. The O−H stretching modes ν(O−H_a) and ν(O−H_b) are localized at 3612 and 3105 cm^{-1}, respectively, and the corresponding bending modes at 740 and 943 cm^{-1}. The new hydroxyl band we calculated at 3612 cm^{-1} has also been observed by Topsøe *et al.*[58,59] and R. C. Adams *et al.*[60] around 3650−3700 cm^{-1}, through the SCR reaction pathway. It was

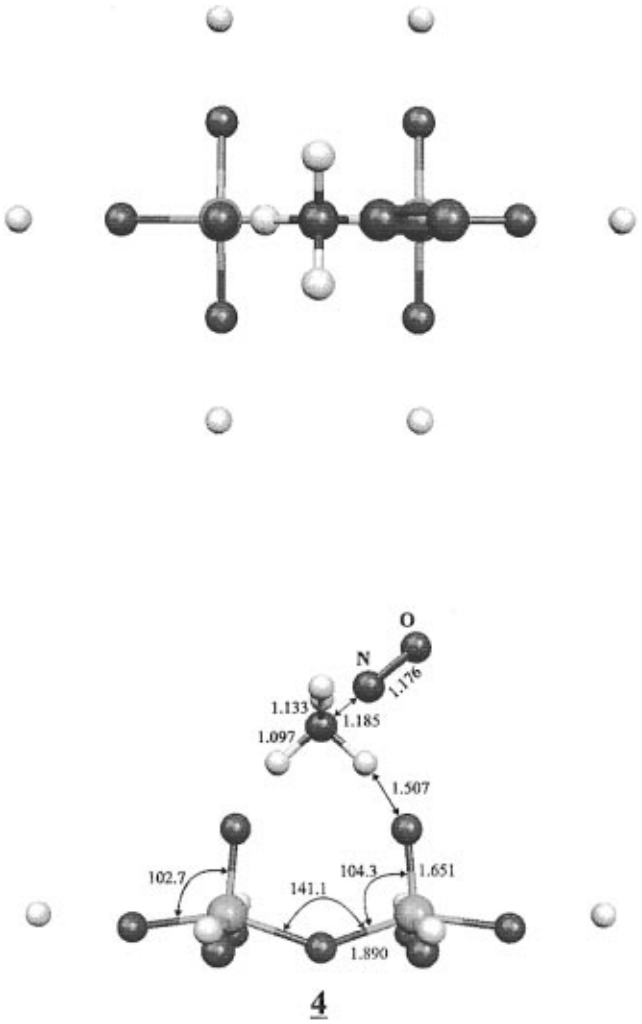

Figure 6. Initial geometry **4** used to model NO reacting with **2a**. Distances are in angstroms and valence angles in degrees.

assigned as a hydroxyl on a reduced vanadium center, V^{+4}−OH, in perfect agreement with the present calculations.

The calculation of the transition state for this reaction turned out to be an intricate task, and no convergence could be achieved using the Gaussian-94/DFT package. However, the barrierless association of NH_2 with NO[21] prompted us to concentrate on a further aspect of the SCR mechanism. Portions of the potential energy surface of the dissociation reaction of NH_2NO were characterized by three different gradient corrected methods, i.e. B3LYP, BPW91, and BP86. The results are displayed in Tables 5−8, and the structures of both intermediates and transition states are illustrated in Figure 9. A schematic potential energy diagram of the NH_2NO dissociation reaction is shown in Figure 10. The qualitative mechanism emerging from these calculations proceeds initially with the association of an adsorbed ammonia with NO to form a highly energized NH_2NO (**lm.1**) adduct, which can undergo a 1,3 H atom migration (**ts.1**), yielding an HNNOH species (**lm.2**), again with considerable excess internal energy. This species, which has a trans conformation with respect to the NN bond and a cis conformation concerning the NO bond, must isomerize to a cis conformation of the NN bond and a trans conformation (**lm.5**) of the NO bond before it can undergo a second 1,3 H atom migration, yielding N_2 and H_2O products. These isomerizations can take place in either order. Isomerization around the NO bond (**ts.2**) is performed by simple torsional rotation (**lm.3**), while isomerization around the NN bond (**lm.4**) occurs by passage through a linear HNN transition state (**ts.3**). The concerted molecular H_2 elimination from the cis−cis HNNOH complex (**lm.4**) yields

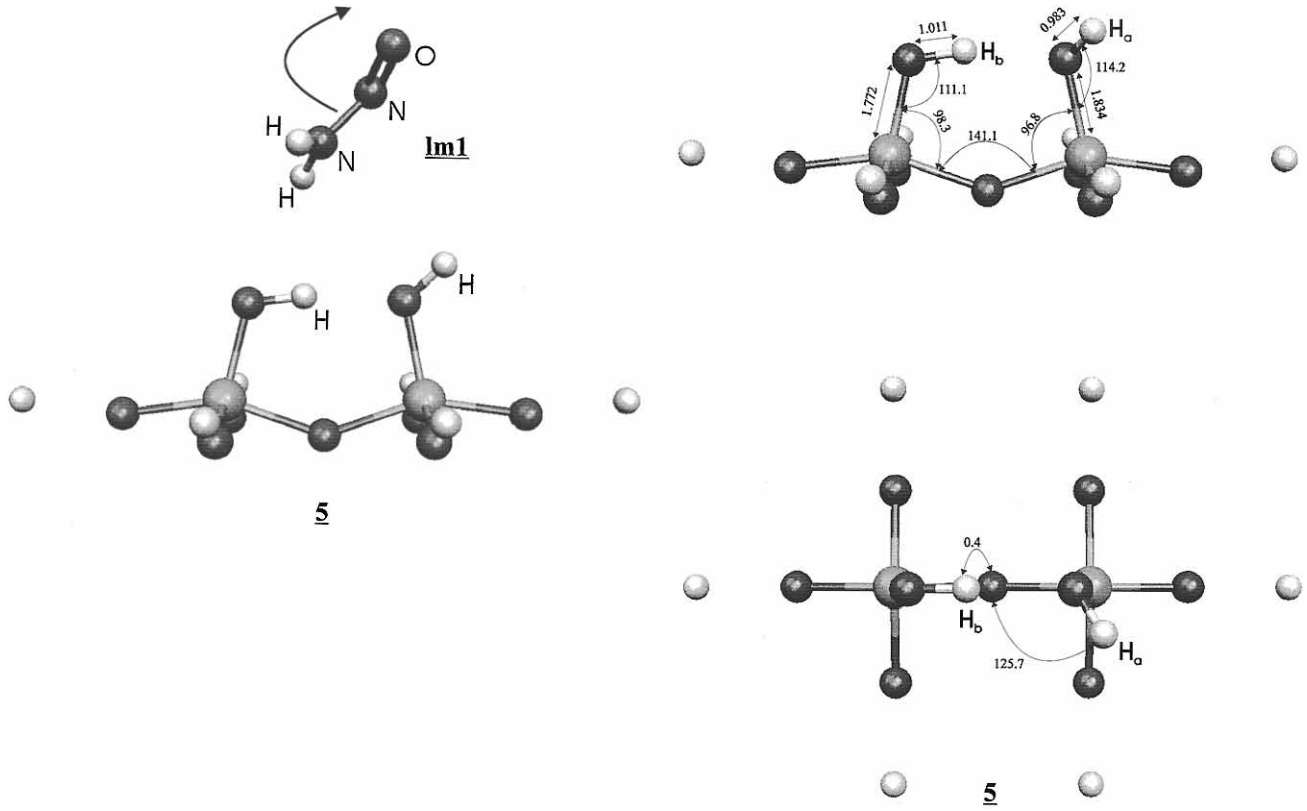

Figure 7. (a, left) Model of the reaction between adsorbed NH_3 with NO, releasing the moiety **5**. (b, right) Structure of **5**.

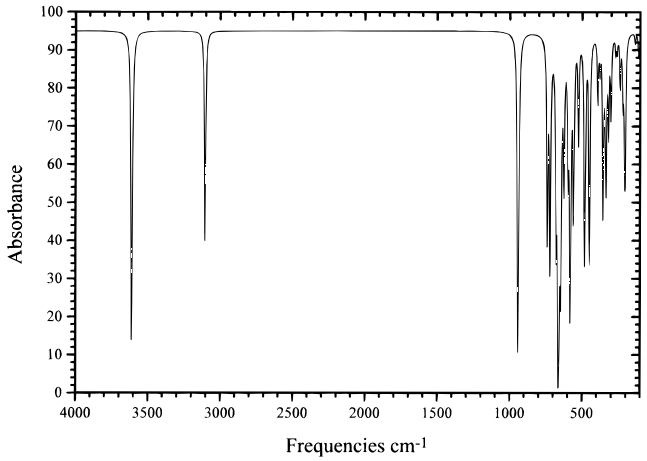

Figure 8. Simulated infrared spectrum of **5**.

$H_2 + N_2O$. The high activation energy, about 30−40 kcal/mol (Table 7), probably results from the inability of the system to exhibit a linear arrangement of the N_2O fragment while keeping the two H atoms in close proximity. The bond lengths derived by the BPW91 and BP86 exchange−correlation functionals are very similar for the stationary points. The absolute mean deviation between the results deduced from these two functionals is about +0.002 Å. On the other hand, the B3LYP functional leads to shorter bond lengths as compared with BPW91. The mean deviations vary from −0.012 Å for δ(N−N), δ(O−H), and δ(N−H) to −0.024 Å for δ(O−N). The same trend is observed for the transition state geometries, but in this case, the mean deviation for δ(O−N) is larger (−0.054 Å). The valence bond angles calculated by B3LYP differ significantly from those deduced from BP86 and BPW91 (−1.0°). The absolute deviation increases to 2.0° for α(N−N−H) for linear HNN transition states (**ts.3** and **ts.5**). The dihedral angles are equivalent whatever exchange−correlation functionals are used.

The relative energies of intermediates and transition states are listed in Table 7. Again, the BPW91 and BP86 functionals lead to similar results with a mean deviation close to 0.5 kcal/mol. On the other hand, the energy barriers derived by using the B3LYP functional are higher by an amount of 2−5 kcal/mol. The discrepancy increases to 8 kcal/mol for the energy of the overall reaction $NH_2NO \rightarrow N_2 + H_2O$.

DF methods yield vibrational frequencies that are consistently closer to experiment than those obtained with the Hartree−Fock (HF) and MP*n* methods. There is an improvement in going from the nonlocal functionals to the hybrid density functional methods.[54,55] The latter lead to harmonic frequencies that are between those calculated with HF (largely overestimated) and MP*n*, and *pure* DF methods.[61−64] The computed harmonic frequencies for the intermediates are displayed in Table 8. The BPW91 and BP86 functionals lead again to similar results for ν(NN) and ν(NO) but are slightly different for ν(NH) and ν(OH). The frequencies derived by using the B3LYP functional are higher and drastically different. In this case, the mean deviations vary from 60 cm^{-1} for ν(NN) and ν(NO) to 120 cm^{-1} for ν(NH) and ν(OH) as compared to that estimated by BPW91.

Finally, the mechanism suggested from the above calculations is in accordance with isotopic labeling studies[15,57] and ^{13}N positron emission,[20] which revealed that in SCR over vanadia-based catalysts N_2 is primarily formed by a nitrogen atom originating from nitric oxide and one from ammonia. The relevance of the mechanism studied by considering a dimeric cluster model mimicking the active sites of a vanadium pentoxide surface certainly has its limitations. Although possible influences due to the presence of the support or promotors are not taken into account, comparative catalytic studies performed on titania-supported vanadia and unsupported vanadia revealed a similar catalytic behavior at temperatures up to 350 °C. Thus it seems that the reaction mechanism governing on pure vanadia is also relevant for (titania)-supported vanadia and consequently for the vanadia-based catalysts used in industrial applications.

TABLE 5: Structural Parameters (Å and deg) of Intermediates in the Dissociation Reaction of NH_2NO Calculated Using the Gaussian-94/DFT Program Package and the B3LYP, PW91, and the BP86 Exchange−Correlation Functionals

	δ-(H−O)	δ-(O−N)	δ-(N−N)	δ-(N−H1)	δ-(N−H2)	α-(H−O−N)	α-(O−N−N)	α-(N−N−H1)	α-(N−N−H2)	α-(H−O−N−N)	α-(O−N−N−H1)	α-(O−N−N−H2)
lm.1		1.222[a]	1.331[a]	1.019[a]	1.009[a]		114.2[a]	119.1[a]	116.9[a]		0.1[a]	179.9[a]
		1.233[b]	1.345[b]	1.027[b]	1.016[b]		114.0[b]	120.3[b]	116.9[b]		0.1[b]	179.9[b]
		1.235[c]	1.347[c]	1.029[c]	1.018[c]		113.9[c]	120.2[c]	116.9[c]		0.1[c]	179.8[c]
lm.2	0.983[a]	1.367[a]	1.236[a]	1.027[a]		106.6[a]	112.0[a]	106.2[a]		0.0[a]		180.0[a]
	0.994[b]	1.377[b]	1.250[b]	1.034[b]		105.9[b]	111.6[b]	105.5[b]		0.0[b]		180.0[b]
	0.997[c]	1.379[c]	1.251[c]	1.037[c]		105.7[c]	111.5[c]	105.4[c]		0.0[c]		180.0[c]
lm.3	0.970[a]	1.393[a]	1.231[a]	1.028[a]		103.0[a]	109.5[a]	104.9[a]		180.0[a]		180.0[a]
	0.978[b]	1.410[b]	1.243[b]	1.035[b]		101.9[b]	109.0[b]	104.1[b]		180.0[b]		180.0[b]
	0.981[c]	1.413[c]	1.244[c]	1.038[c]		101.8[c]	108.9[c]	104.0[c]		180.0[c]		180.0[c]
lm.4	0.983[a]	1.394[a]	1.226[a]	1.043[a]		109.4[a]	118.4[a]	113.5[a]		0.0[a]		0.0[a]
	0.993[b]	1.411[b]	1.236[b]	1.052[b]		108.6[b]	118.6[b]	113.6[b]		0.0[b]		0.0[b]
	0.995[c]	1.413[c]	1.237[c]	1.055[c]		108.5[c]	118.6[c]	113.5[c]		0.0[c]		0.0[c]
lm.5	0.971[a]	1.428[a]	1.221[a]	1.039[a]		103.8[a]	112.4[a]	111.5[a]		180.0[a]		0.0[a]
	0.979[b]	1.452[b]	1.229[b]	1.048[b]		102.7[b]	112.5[b]	111.9[b]		180.0[b]		0.0[b]
	0.981[c]	1.455[c]	1.231[c]	1.049[c]		102.7[c]	112.4[c]	111.8[c]		180.0[c]		0.0[c]

[a] B3LYP. [b] PW91. [c] BP86.

TABLE 6: Structural Parameters (Å and deg) of Transition States in the Dissociation Reaction of NH_2NO Calculated Using the B3LYP, PW91, and the BP86 Exchange−Correlation Functionals

	δ(H−O)	δ(O−N)	δ(N−N)	δ(N−H)	α(H−O−N)	α(O−N−N)	α(N−N−H)	α(H−O−N−N)	α(O−N−N−H)
ts.1	1.354[a]	1.291[a]	1.273[a]	1.021[a]	78.3[a]	102.9[a]	117.9[a]	0.0[a]	180.0[a]
	1.365[b]	1.302[b]	1.286[b]	1.029[b]	78.3[b]	102.7[b]	117.5[b]	0.0[b]	180.0[b]
	1.369[c]	1.303[c]	1.288[c]	1.031[c]	78.4[c]	102.8[c]	117.4[c]	0.0[c]	180.0[c]
ts.2	0.972[a]	1.438[a]	1.225[a]	1.032[a]	105.2[a]	109.8[a]	105.0[a]	86.8[a]	177.4[a]
	0.979[b]	1.460[b]	1.235[b]	1.041[b]	104.2[b]	109.2[b]	104.3[b]	87.0[b]	177.2[b]
	0.982[c]	1.463[c]	1.237[c]	1.043[c]	104.1[c]	109.2[c]	104.2[c]	87.0[c]	177.2[c]
ts.3	0.979[a]	1.484[a]	1.193[a]	0.998[a]	105.9[a]	114.8[a]	178.1[a]	0.0[a]	180.0[a]
	0.986[b]	1.551[b]	1.197[b]	1.004[b]	104.6[b]	114.9[b]	176.2[b]	0.0[b]	180.0[b]
	0.989[c]	1.551[c]	1.199[c]	1.006[c]	104.5[c]	114.8[c]	176.2[c]	0.0[c]	180.0[c]
ts.4	0.973[a]	1.469[a]	1.217[a]	1.040[a]	105.7[a]	114.8[a]	112.7[a]	67.7[a]	−0.1[a]
	0.981[b]	1.508[b]	1.223[b]	1.048[b]	104.0[b]	114.1[b]	113.0[b]	70.8[b]	−0.2[b]
	0.983[c]	1.510[c]	1.224[c]	1.051[c]	104.0[c]	114.0[c]	112.9[c]	70.5[c]	−0.2[c]
ts.5	0.972[a]	1.551[a]	1.178[a]	0.997[a]	101.5[a]	110.9[a]	174.3[a]	180.0[a]	180.0[a]
	0.981[b]	1.613[b]	1.184[b]	1.024[b]	99.9[b]	110.8[b]	172.5[b]	180.0[b]	180.0[b]
	0.982[c]	1.613[c]	1.186[c]	1.004[c]	99.9[c]	110.8[c]	172.6[c]	180.0[c]	180.0[c]
ts.6	0.973[a]	1.850[a]	1.164[a]	1.136[a]	141.7[a]	88.9[a]	104.4[a]	180.0[a]	0.0[a]
	0.983[b]	1.924[b]	1.170[b]	1.140[b]	139.5[b]	88.8[b]	103.3[b]	180.0[b]	0.0[b]
	0.984[c]	1.924[c]	1.171[c]	1.120[c]	139.5[c]	88.8[c]	103.4[c]	180.0[c]	0.0[c]
ts.7	1.450[a]	1.250[a]	1.183[a]	1.466[a]	89.2[a]	127.6[a]	92.2[a]	0.0[a]	0.0[a]
	1.475[b]	1.254[b]	1.198[b]	1.442[b]	88.8[b]	127.6[b]	93.0[b]	0.0[b]	0.0[b]
	1.478[c]	1.256[c]	1.199[c]	1.450[c]	88.1[c]	127.1[c]	92.9[c]	0.0[c]	0.0[c]

[a] B3LYP. [b] PW91. [c] BP86.

TABLE 7: Relative Energies (kcal/mol) of Intermediates and Transition States in the Dissociation Reaction of NH_2NO Calculated Using the B3LYP, PW91, and the BP86 Exchange−Correlation Functionals

	B3LYP	B3LYP-ZPEC[a]	PW91	PW91-ZPEC[a]	BP86	BP86-ZPEC[a]
NH_2NO	0.00	0.00	0.00	0.00	0.00	0.00
lm.2	2.85	2.33	3.75	3.28	3.41	2.94
lm.3	3.67	3.07	4.67	4.08	4.41	3.81
lm.4	10.08	10.42	10.09	10.53	9.68	10.11
lm.5	3.03	2.99	3.49	3.51	3.11	3.13
ts.1	32.30	35.04	27.95	30.63	27.29	29.94
ts.2	12.54	13.11	14.49	15.12	14.15	14.76
ts.3	38.93	41.31	36.76	39.36	36.34	38.91
ts.4	13.34	14.38	14.17	15.31	13.73	14.86
ts.5	35.66	37.87	33.25	35.52	32.90	35.14
ts.6	24.20	29.77	22.12	27.54	21.10	26.62
ts.7	50.85	56.11	43.31	48.24	42.26	47.33
$N_2 + H_2O$	−62.47	−66.05	−55.47	−58.79	−54.17	−57.46
$N_2O + H_2$	10.96	3.85	6.36	0.36	7.90	1.21

[a] Including the zero-point vibrational energies correction.

IV. Conclusion

Quantum chemical calculations carried out on a V_2O_9H model cluster support earlier experimental findings which indicated that the vanadium oxide-catalyzed SCR of NO is initiated by NH_3 adsorption on a Brønsted acid site. The adsorbed NH_3 is activated by transferring an H to the V^{5+}═O site, which becomes partly reduced. Gaseous or weakly adsorbed NO subsequently reacts with this activated NH_3, leading to the formation of V^{4+}−OH and NH_2NO. The NH_2NO species is not observed experimentally under SCR conditions, because it undergoes rapid decomposition, yielding the reaction products N_2 and H_2O. In order to complete the catalytic cycle, V^{4+}−OH must be oxidized to V^{5+}═O. The theoretical findings that

TABLE 8: Vibrational Frequencies (cm^{-1}) of Intermediates in the Dissociation Reaction of NH_2NO Calculated using the B3LYP, PW91, and the BP86 Exchange−Correlation Functionals

	ω_1	ω_2	ω_3	ω_4	ω_5	ω_6	ω_7	ω_8	ω_9
lm.1[d]	242[a]	628[a]	712[a]	1110[a]	1226[a]	1581[a]	1606[a]	3472[a]	3710[a]
	241[b]	594[b]	701[b]	1039[b]	1177[b]	1523[b]	1546[b]	3366[b]	3623[b]
	235[c]	592[c]	699[c]	1033[c]	1173[c]	1515[c]	1537[c]	3342[c]	3601[c]
lm.2[e]	653[a]	665[a]	944[a]	957[a]	1361[a]	1435[a]	1647[a]	3428[a]	3565[a]
	638[b]	662[b]	906[b]	909[b]	1309[b]	1390[b]	1567[b]	3339[b]	3415[b]
	636[c]	661[c]	901[c]	905[c]	1303[c]	1383[c]	1559[c]	3317[c]	3388[c]
lm.3[e]	507[a]	665[a]	911[a]	965[a]	1328[a]	1437[a]	1689[a]	3416[a]	3789[a]
	516[b]	638[b]	855[b]	927[b]	1279[b]	1391[b]	1610[b]	3330[b]	3677[b]
	513[c]	636[c]	850[c]	923[c]	1273[c]	1385[c]	1602[c]	3308[c]	3656[c]
lm.4[e]	488[a]	649[a]	870[a]	957[a]	1279[a]	1404[a]	1683[a]	3166[a]	3557[a]
	509[b]	600[b]	809[b]	922[b]	1229[b]	1340[b]	1615[b]	3061[b]	3420[b]
	508[c]	599[c]	806[c]	917[c]	1223[c]	1334[c]	1607[c]	3034[c]	3393[c]
lm.5[e]	463[a]	613[a]	803[a]	1008[a]	1280[a]	1386[a]	1729[a]	3256[a]	3782[a]
	472[b]	569[b]	740[b]	968[b]	1225[b]	1319[b]	1664[b]	3164[b]	3673[b]
	467[c]	567[c]	736[c]	964[c]	1217[c]	1313[c]	1657[c]	3138[c]	3650[c]

[a] B3LYP. [b] PW91. [c] BP86. [d] ω_1, $\gamma(NH_2)$; ω_2, $\rho(NH_2)$; ω_4, $\nu(NN)$; ω_5, $\rho(NH_2)$; ω_6, $\delta(NH_2)$; ω_7, $\nu(NO)$; ω_8, $\nu_{sym}(NH)$; ω_9, $\nu_{asym}(NH)$. [e] ω_4, $\nu(NO)$; ω_7, $\nu(NN)$; ω_8, $\nu(NH)$; ω_9, $\nu(OH)$.

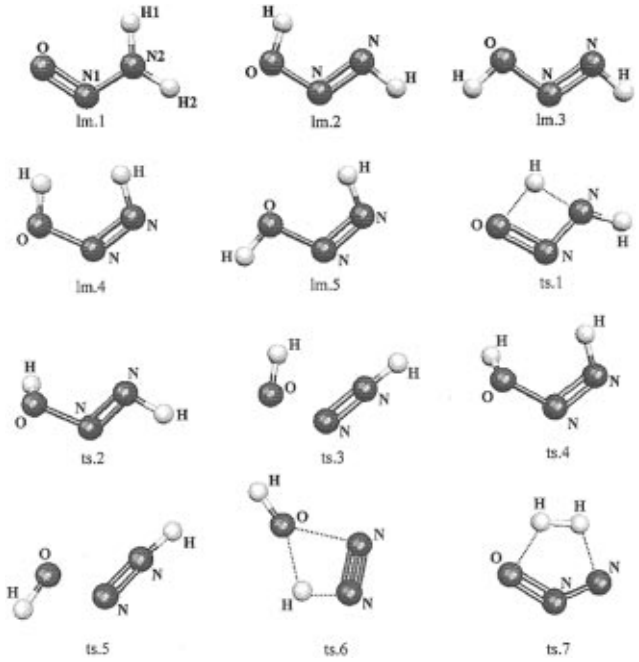

Figure 9. Structures of several intermediates and transition states in the dissociation reaction of NH_2NO.

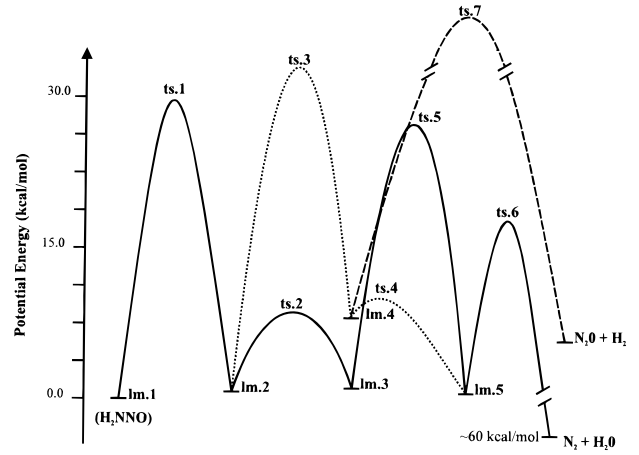

Figure 10. Relative energies of intermediates and transition states in the dissociation reaction of NH_2NO.

emerged from our DFT modeling of the SCR reaction are in agreement with an Eley−Rideal-type mechanism. They provide a detailed analysis of the energetical and structural characteristics of the reaction between activated NH_3 and NO.

Acknowledgment. Financial Support by the Swiss National Science Foundation is kindly acknowledged.

References and Notes

(1) Bosch, H.; Janssen, F. *Catal. Today* **1987**, *2* (4), 369. Bond, G. C.; Tahir, S. F. *Appl. Catal.* **1991**, *71* (1).
(2) Takagi, M.; Kawai, T.; Soma, M.; Onishi, T.; Tamuru, T. *J. Catal.* **1977**, *50*, 441.
(3) Inomata, M.; Miyamoto, A.; Murakami, Y. *J. Catal.* **1980**, *62*, 140.
(4) Gasior, M.; Haber, J.; Machej, T.; Czeppe, T. *J. Mol. Catal.* **1988**, *43*, 359.
(5) Rajadhyaksha, R. A.; Knözinger, H. *Appl. Catal.* **1989**, *51*, 81.
(6) Odriozola, J. A.; Heineman, H.; Somorjai, G. A.; De la Banda, J. F.; Pereira, P. *Appl. Catal.* **1989**, *119*, 71.
(7) Ramis, G.; Busca, G.; Lorenzelli, V.; Forzatti, P. *Appl. Catal.* **1990**, *64*, 243.
(8) Schraml, M.; Wokaum, A.; Baiker, A. *J. Catal.* **1990**, *124*, 86.
(9) Topsøe, N. Y. *J. Catal.* **1991**, *128*, 499.
(10) Went, G. T.; Leu, L.-J.; Rosin, R. R.; Bell, A. T. *J. Catal.* **1992**, *134*, 492.
(11) Dumesic, J. A. In *New Frontiers in Catalysis*, Proceedings of the 10th International Congress on Catalysis, Budapest, Hungary; Guczi, L., *et al.*, Eds.; Akadémiai Kadó: Budapest, 1993; p 1325.
(12) Schneider, H.; Tschudin, S.; Schneider, M.; Wokaun, A.; Baiker, A. *J. Catal.* **1994**, *147*, 5.
(13) Ramis, G.; Busca, G.; Lorenzelli, V.; Forzatti, P. *Appl. Catal.* **1990**, *64*, 259.
(14) Takagi, M.; Kawai, T.; Soma, M.; Onishi, T.; Tamuru, T. *J. Phys. Chem.* **1976**, *80*, 430.
(15) Janssen, F. J. J. G.; van den Kerkhof, F. M. G.; Bosch, H.; Ross, J. R. H. *J. Phys. Chem.* **1987**, *91*, 5921.
(16) Topsøe, N.-Y.; Topsøe, H. *Catal. Today* **1991**, *9*, 77. Topsøe, N.-Y. *Science* **1994**, *265*, 1217.
(17) Schneider, H.; Tschudin, S.; Schneider, M.; Wokaum, A.; Baiker, A. *J. Catal.* **1994**, *147*, 5.
(18) Topsøe, N.-Y.; Salbiak, T.; Clausen, S. B.; Srnak, T. Z.; Dumesic, J. A. *J. Catal.* **1992**, *134*, 742.
(19) Srnak, T. Z.; Dumesic, J. A.; Clausen, B. S.; Törnqvist, E.; Topsøe, N.-Y. *J. Catal.* **1992**, *135*, 246.
(20) Baltensperger, U.; Amman, M.; Bochert, U.; Eichler, B.; Gäggeler, H. W.; Jost, D.; Kovacs, J.; Türler, A.; Scherer, U. W.; Baiker, A. *J. Phys. Chem.* **1995**, *97*, 12325.
(21) Duan, X.; Page, M. *J. Mol. Struct.* (*THEOCHEM*) **1995**, *333*, 233.
(22) Kulkarni, S. A.; Pundnik, S. S. *Chem. Phys. Lett.* **1995**, *245*, 143.
(23) Diau, E. R.-W.; Smith, S. C. *J. Phys. Chem.* **1996**, *100*, 12349.
(24) Walch, S. P. *J. Chem. Phys.* **1993**, *99*(7), 5295.
(25) Bradley, K. S.; McCabe, P.; Schatz, G. C.; Walch, S. P. *J. Chem. Phys.* **1995**, *102*(17), 6696.
(26) Koizumi, H.; Schatz, G. C.; Walch, S. P. *J. Chem. Phys.* **1991**, *95*, 4130.
(27) Wolf, M.; Yang, D. L.; Durant, J. L. *J. Photochem. Photobiol. A: Chem.* **1994**, *80*, 85.
(28) Durant, J. L., Jr. In *Reactions of NHx Species, Research in Chemical Kinetics, Vol. 3*; Compton, R. G., Hancock, G., Eds.; Elsevier Science B.V.: Amsterdam, 995; pp 69−115.
(29) Melius, C. F.; Binkley, J. S. *Symp. (Int.) Combust. Proc.* **1984**, *20*, 575.
(30) Casewit, C. J.; Goddard, W. A. *J. Am. Chem. Soc.* **1982**, *104*, 3280.
(31) Abou-Rachid, H.; Pouchan, C.; Chaillet, M. *Chem. Phys.* **1984**, *90*, 243.

(32) Harrison, J. A.; Maclagan, G. A. R.; White, A. R. *J. Phys. Chem.* **1987**, *91*, 6683.
(33) Gilardoni, F.; Weber, J.; Baiker, A. *Int. J. Quantum Chem.* **1997**, *61*, 683−688.
(34) Witko, M.; Hermann, K. *J. Mol. Catal.* **1993**, *81*, 279.
(35) Hermann, K.; Bagus, P. S. *Phys. Rev.* **1978**, *B17*, 4082.
(36) Witko, M.; Tokarz, R.; Haber, J. *J. Mol. Catal.* **1991**, *66*, 205.
(37) Petelenz, P.; Broclawik, E. *J. Mol. Catal.* **1991**, *68*, 223; *Ibid*. **1993**, *80*, 341.
(38) Nalewajjski, R. F. *J. Mol. Catal.* **1993**, *82*, 371.
(39) Kobayashi, H.; Yamaguchi, M.; Tanaka, T.; Nishimura, Y.; Kawakami, Y. H.; Yoshida, S. *J. Phys. Chem.* **1988**, *92*, 2516.
(40) Efstathiou, A. M.; Fliatoura, K. *Appl. Catal., B* **1995**, 6.
(41) Andzelm, J.; Radzio, E.; Salahub, D. R. *J. Chem. Phys.* **1985**, *83*, 4573.
(42) Salahub, D. R. In *Applied Quantum Chemistry*; Smith, V. H., Schafer, H. F., Morokuma, K., Eds.; Reidel: Dordrecht, 1986; p 185.
(43) Salahub, D. R. *Adv. Chem. Phys.* **1987**, *69*, 447.
(44) Salahub, D. R.; Fournier, R.; Mlynarski, P.; Papai, I.; St-Amant, A.; Ushio, J. In *Density Functional Methods in Chemistry*; Labanowski, K., Andzelm, J., Eds.; Springer: New York, 1991; p 77.
(45) Becke, A. D. *J. Chem. Phys.* **1988**, *88*, 2457. Becke, A. D. *Phys. Rev. A.* **1988**, *38*, 3098.
(46) Perdew, J. P. *Phys. Rev. B* **1986**, *33*, 8822; **1986**, *34*, 7046.
(47) Godbout, N.; Salahub, D. R.; Andzelm, J.; Wimmer, E. *Can. J. Chem.* **1992**, *70*, 560.
(48) Frisch, M. J.; Trucks, G. W.; Schlegel, H. B.; Gill, P. M. W.; Johnson, B. G.; Wong, M. W.; Foresman, J. B.; Robb, M. A.; Head-Gordon, M.; Replogle, E. S.; Gomperts, R.; Andres, J. L.; Raghavachari, K.; Binkley, J. S.; Gonzales, C.; Martin, R. L.; Fox, D. J.; Defrees, D. J.; Baker, J.; Stewart, J. P. P.; Pople, J. A. *Gaussian 94/DFT*, revision F4; Gaussian, Inc.: Pittsburgh, PA 1995.
(49) Becke, A. D. *J. Chem. Phys.* **1993**, *98*, 5648.
(50) Lee, C.; Yang, W.; Parr, R. G. *Phys. Rev. B* **1988**, *37*, 785.
(51) Miehlich, B.; Savin, A.; Stoll, H.; Preuss, H. *Chem. Phys. Lett.* **1989**, *157*, 200.
(52) Perdew, J. P.; Wang, Y. *Phys. Rev.* **1992**, *B45*, 13244.
(53) Rauhut, G.; Pulay, P. *J. Phys. Chem.* **1995**, *99*, 3093.
(54) Zhou, X.; Wheeless, C. J. M.; Liu, R. *Vib. Spectrosc.* **1996**, *12*, 53−63.
(55) Wong, M. W. *Chem. Phys. Lett.* **1996**, *256*, 391−399.
(56) Farber, M.; Harris, S. P. *J. Chem. Phys.* **1984**, *88*, 680.
(57) Duffy, B. L.; Curry-Hyde, H. E.; Cant, N. W.; Nelson, P. F. *Catal. Lett*. **1994**, *28*, 167.
(58) Topsøe, N.-Y.; Topsøe, H.; Dumesic, J. *J. Catal*. **1995**, *151*, 226.
(59) Topsøe, N.-Y.; Topsøe, H.; Dumesic, J. *J. Catal*. **1995**, *151*, 241.
(60) Adams, R. C.; Xu, L.; Moller, K.; Bein, T.; Delgass, W. N. *Catal. Today* **1997**, *33*, 263−278.
(61) Pople, J. A.; Scott, A. P.; Wong, M. W.; Israel, L. R. *J. Chem.* **1993**, *33*, 345.
(62) Hout, R. F.; Levi, B. A.; Hehre, W. J. *J. Comput. Chem.* **1982**, *3*, 234.
(63) DeFrees, D. J.; McLean, A. D. *J. Chem. Phys.* **1985**, *82*, 333.
(64) Latajka, Z.; Bouteiller, Y. *J. Chem. Phys.* **1994**, *101*, 119.